# TIME-DELAYED DYNAMIC OUTPUT FEEDBACK $\mathcal{H}_\infty$ CONTROLLER DESIGN FOR CIVIL STRUCTURES: A DECENTRALIZED APPROACH THROUGH HOMOTOPIC TRANSFORMATION

**Yang Wang**

School of Civil and Environmental Engineering, Georgia Institute of Technology
790 Atlantic Dr NW, Atlanta, GA 30332-0355

**Abstract** For the control of large-scale complex systems, it has been widely recognized that decentralized approaches may offer a number of advantages compared with centralized approaches. Primarily, these advantages include less feedback latency and lower demand on communication range, which may result in better control performance and lower system cost. This paper presents a decentralized approach for the control of large-scale civil structures. The approach provides decentralized dynamic output feedback controllers that minimize the $\mathcal{H}_\infty$ norm of the closed-loop system. The effect of feedback time delay is considered in the problem formulation, and therefore, compensated during the controller design. The control decentralization is achieved using a homotopy method that gradually transforms a typical centralized controller into multiple uncoupled decentralized controllers. At each homotopy step, linear matrix inequality (LMI) constraints are satisfied to guarantee the performance requirement for the closed-loop $\mathcal{H}_\infty$ norm. The proposed algorithm is validated through numerical simulations with a five-story example structure. Performance of the proposed algorithm is compared with a time-delayed decentralized control algorithm that is based upon the linear quadratic regulator (LQR) criteria.

**Keywords**: structural control, feedback time delay, decentralized control, H-infinity control, homotopy method, linear matrix inequality.

## 1. Introduction

Over the last few decades, real-time feedback structural control has attracted a great amount of interest in the structural engineering community [1-4]. For example, it was reported that about 50 buildings and towers had been instrumented with various types of structural control systems from 1989 to 2003 [5]. A feedback structural control system contains a network of sensors, controllers, and actuators. Components in this network collaboratively mitigate structural vibration when strong external excitations (such as earthquakes or typhoons) occur. When the excitation begins, dynamic responses of the structure are measured by sensors in real time. Sensor data are immediately communicated to a controller, which makes appropriate control decisions and dispatches the decisions to structural control devices. The control devices then apply corresponding forces to the structure to counter-balance the effects due to external excitation, so that excessive structural vibration is mitigated. Typical control devices for feedback structural control include semi-active hydraulic dampers (SHD), magnetorheological (MR) dampers, active mass dampers (AMD), etc. Semi-active control devices are currently

preferred by many researchers and engineers, because of their power efficiency, inherent stability, and adaptability in real-time feedback control [6].

Traditional structural feedback control systems adopt centralized communication schemes. In such a system, one central controller collects data from all the sensors in the structure. The controller then makes control decisions, and delivers commands to all the structural control devices so that appropriate forces can be generated to mitigate structural vibration. In a centralized control system, requirements on communication range and data transmission rate increase rapidly with the structural size and the number of sensors and actuators being deployed. These communication requirements could result in considerable economical and technical difficulties for implementation in large-scale civil structures, such as high-rise buildings with hundreds of stories. Furthermore, the centralized controller represents a point of potential bottleneck failure for the whole system.

In order to resolve these inherent problems of a centralized control system, decentralized control strategies can be explored [7-9]. For decentralized control, a large-scale control system is divided into a collective set of smaller and distributed sub-systems. In each subsystem, decentralized controllers require only local and neighboring sensor data to make control decisions, and command only control devices in the vicinity. As a result, higher control sampling rates and less feedback time delay can be offered by decentralized control; furthermore, shorter communication range and lower data transmission rate are required. On the other hand, because each decentralized controller only has local and neighboring sensor data available for control decisions, decentralized control systems may only achieve sub-optimal control performance when compared to centralized systems. Therefore, decentralized controllers need to be designed with special consideration.

Decentralized structural controller design based on the linear quadratic regulator (LQR) optimization criteria has been studied [10]. The design provides static output feedback controllers which consider the effect of feedback time delay. This paper explores a different control methodology, namely the $\mathcal{H}_\infty$ control theory that can offer excellent control performance when "worst-case" external disturbances are encountered. Centralized $\mathcal{H}_\infty$ controller design in the continuous-time domain for civil structural control has been studied by researchers [11-17]. Their work illustrates the feasibility and effectiveness of centralized $\mathcal{H}_\infty$ control for civil structures. For example, it has been shown that $\mathcal{H}_\infty$ control design may achieve excellent performance in attenuating transient vibrations of structures [18]. However, decentralized $\mathcal{H}_\infty$ controller design that considers feedback time delay has rarely been explored by the community.

The performance objective for $\mathcal{H}_\infty$ controller design can be formulated using linear matrix inequalities (LMI) [19]. For an optimization problem with LMI constraints, sparsity patterns can be easily applied to the matrix variables. This property offers great convenience for designing decentralized controllers where sparsity patterns in the parametric controller matrices can represent decentralized information feedback. A preliminary study on decentralized $\mathcal{H}_\infty$ controller design, which is based on static state feedback, has been performed [20]. In the preliminary work, controller gain matrices that are block-diagonal or close to block-diagonal can

represent various decentralized feedback patterns, where only neighboring sensor data is required for determining optimal control forces. This study, however, cannot consider feedback time delay in the controller design. Since feedback time delay inevitably exists in a practical structural control system, the inability to consider time delay during controller design may result in significant performance degradation, or even destabilize the structure in case of an active control system. Because the previous $\mathcal{H}_\infty$ controller design cannot be easily extended to provide controllers that utilize measurement output feedback (instead of state feedback), or controllers that can effectively consider feedback time delay, a new approach is developed in this work.

This paper proposes a decentralized $\mathcal{H}_\infty$ structural controller design that provides dynamic output feedback controllers. The control problem is formulated in discrete-time domain so that feedback time delay can be effectively considered. A homotopy method for designing decentralized $\mathcal{H}_\infty$ controllers in continuous-time domain, which was described by Zhai, *et al.* [21], is adapted for this research. The method gradually transforms a centralized controller into uncoupled decentralized ones that correspond to certain decentralized feedback patterns. LMI constraints describing the closed-loop $\mathcal{H}_\infty$ norm performance are guaranteed at each homotopy step.

This paper first describes the formulation of multiple dynamical systems involved in the controller design. The homotopy method that computes decentralized $\mathcal{H}_\infty$ controllers is then described. A five-story structure is adopted in the numerical validations that demonstrate the performance of the time-delayed decentralized $\mathcal{H}_\infty$ controller design. Performance of the proposed decentralized $\mathcal{H}_\infty$ controller design is compared with a previously presented time-delayed decentralized controller design, which is based on LQR optimization criteria [10].

## 2. Problem Formulation

For a lumped-mass structural model with $n$ degrees-of-freedom (DOF) and instrumented with $n_u$ control devices, the equations of motion can be formulated as:

$$\mathbf{M}\ddot{\mathbf{q}}(t)+\mathbf{C}\dot{\mathbf{q}}(t)+\mathbf{K}\mathbf{q}(t)=\mathbf{T}_{\mathbf{w}_1}\mathbf{w}_1(t)+\mathbf{T}_{\mathbf{u}}\mathbf{u}(t) \tag{1}$$

where $\mathbf{q}(t) \in \mathbb{R}^{n\times 1}$ is the displacement vector relative to the ground; $\mathbf{M}$, $\mathbf{C}$, $\mathbf{K} \in \mathbb{R}^{n\times n}$ are the mass, damping, and stiffness matrices, respectively; $\mathbf{w}_1(t) \in \mathbb{R}^{n_{w1}\times 1}$ and $\mathbf{u}(t) \in \mathbb{R}^{n_u\times 1}$ are the external excitation vector and control force vector, respectively; $\mathbf{T}_{\mathbf{w}1} \in \mathbb{R}^{n\times n_{w1}}$ and $\mathbf{T}_{\mathbf{u}} \in \mathbb{R}^{n\times n_u}$ are the external excitation and control force location matrices, respectively.

For brevity, the discussion below is based on a 2-D shear-frame structure subject to unidirectional ground excitation. The same formulation can be easily extended to 3-D structural models. It is assumed that the external excitation $\mathbf{w}_1(t)$ is a scalar ($n_{w1} = 1$), *i.e.* the ground acceleration history $\ddot{q}_g(t)$. Therefore, the spatial load pattern is:

$$\mathbf{T}_{\mathbf{w1}} = -\mathbf{M}\{\mathbf{1}\}_{n\times 1} \tag{2}$$

Entries in $\mathbf{u}(t)$ are defined as the control forces between neighboring floors. The forces can be applied by control devices associated with stiff V-braces that connect two neighboring floors. If a positive control force is defined to be moving the floor above the control device towards the left direction, and moving the floor below the control device towards the right direction, the control force location matrix $\mathbf{T_u}$ is determined as:

$$\mathbf{T_u} = \begin{bmatrix} -1 & 1 & & \\ & \ddots & \ddots & \\ & & -1 & 1 \\ & & & -1 \end{bmatrix} \tag{3}$$

Based upon the equations of motion, the state-space system can be formulated as:

$$\dot{\mathbf{x}}_I(t) = \mathbf{A}_I \mathbf{x}_I(t) + \mathbf{E}_I \mathbf{w}_1(t) + \mathbf{B}_I \mathbf{u}(t) \tag{4}$$

where $\mathbf{x}_I(t) = \left[\mathbf{q}(t); \dot{\mathbf{q}}(t)\right] \in \mathbb{R}^{2n\times 1}$ is the state vector; $\mathbf{A}_I \in \mathbb{R}^{2n\times 2n}$, $\mathbf{E}_I \in \mathbb{R}^{2n\times n_{w1}}$, and $\mathbf{B}_I \in \mathbb{R}^{2n\times n_u}$ are, respectively, the system, excitation influence, and control influence matrices given as follows:

$$\mathbf{A}_I = \begin{bmatrix} [\mathbf{0}]_{n\times n} & [\mathbf{I}]_{n\times n} \\ -\mathbf{M}^{-1}\mathbf{K} & -\mathbf{M}^{-1}\mathbf{C} \end{bmatrix},\ \mathbf{E}_I = \begin{bmatrix} [\mathbf{0}]_{n\times n_{w1}} \\ \mathbf{M}^{-1}\mathbf{T}_{w_1} \end{bmatrix},\ \mathbf{B}_I = \begin{bmatrix} [\mathbf{0}]_{n\times n_u} \\ \mathbf{M}^{-1}\mathbf{T_u} \end{bmatrix} \tag{5}$$

To facilitate the derivation for decentralized control, a linear transformation to the state vector is performed. In the transformed state vector $\mathbf{x}_{II}(t) \in \mathbb{R}^{2n\times 1}$, the displacement and velocity entries at the same story are concatenated together:

$$\mathbf{x}_{II}(t) = [q_1(t) \quad \dot{q}_1(t) \quad q_2(t) \quad \dot{q}_2(t) \quad \ldots \quad q_n(t) \quad \dot{q}_n(t)]^{\mathrm{T}} \tag{6}$$

To obtain the transformed state vector $\mathbf{x}_{II}(t)$, a linear transformation matrix $\mathbf{\Gamma}$ is defined to shuffle the entries in the original state vector $\mathbf{x}_I$:

$$\mathbf{x}_{II}(t) = \mathbf{\Gamma}\mathbf{x}_I(t) \tag{7}$$

Substituting $\mathbf{x}_I(t) = \mathbf{\Gamma}^{-1}\mathbf{x}_{II}(t)$ into Eq. (4), and left-multiplying the equation with $\mathbf{\Gamma}$, the state space representation using the transformed state vector becomes:

$$\dot{\mathbf{x}}_{II}(t) = \mathbf{A}_{II}\mathbf{x}_{II}(t) + \mathbf{E}_{II}\mathbf{w}_1(t) + \mathbf{B}_{II}\mathbf{u}(t) \tag{8}$$

where $\mathbf{A}_{II} = \mathbf{\Gamma}\mathbf{A}_I\mathbf{\Gamma}^{-1}$, $\mathbf{E}_{II} = \mathbf{\Gamma}\mathbf{E}_I$, and $\mathbf{B}_{II} = \mathbf{\Gamma}\mathbf{B}_I$. The controlled output vector $\mathbf{z}(t) \in \mathbb{R}^{n_z\times 1}$ is defined as:

$$\mathbf{z}(t) = \mathbf{C_z}\mathbf{x}_{II}(t) + \mathbf{F_z}\mathbf{w}_1(t) + \mathbf{D_z}\mathbf{u}(t) \tag{9}$$

Similarly, the sensor measurement vector $\mathbf{m}(t) \in \mathbb{R}^{n_m\times 1}$ can be defined in a general form as:

$$\mathbf{m}(t) = \mathbf{C_m}\mathbf{x}_{II}(t) + \mathbf{F_m}\mathbf{w}_1(t) + \mathbf{D_m}\mathbf{u}(t) \tag{10}$$

Using zero-order hold, the continuous-time dynamics in Eq. (8) can be discretized using a sampling period $\Delta T$ [22]. The complete discrete-time structural system, which includes descriptions of the system dynamics, the output, and the measurement, can be summarized as:

$$\begin{cases} \mathbf{x}_S[k+1] = \mathbf{A_d}\mathbf{x}_S[k] + \mathbf{E_d}\mathbf{w}_1[k] + \mathbf{B_d}\mathbf{u}[k] \\ \mathbf{z}[k] = \mathbf{C_z}\mathbf{x}_S[k] + \mathbf{F_z}\mathbf{w}_1[k] + \mathbf{D_z}\mathbf{u}[k] \\ \mathbf{m}[k] = \mathbf{C_m}\mathbf{x}_S[k] + \mathbf{F_m}\mathbf{w}_1[k] + \mathbf{D_m}\mathbf{u}[k] \end{cases} \tag{11}$$

where $k$ represents the discrete time step, and the subscript "d" denotes variables in the discrete-time domain. In Eq. (11), the matrices $\mathbf{A_d}$, $\mathbf{E_d}$, and $\mathbf{B_d}$ are given as:

$$\begin{aligned} \mathbf{A_d} &= e^{\mathbf{A}_{II}\Delta T} \\ \mathbf{E_d} &= \int_0^{\Delta T} e^{\mathbf{A}_{II}\tau}\mathbf{E}_{II}\,d\tau = \mathbf{A}_{II}^{-1}\left(e^{\mathbf{A}_{II}\Delta T} - \mathbf{I}\right)\mathbf{E}_{II}, \text{ when } \mathbf{A}_{II}^{-1} \text{ exists} \\ \mathbf{B_d} &= \int_0^{\Delta T} e^{\mathbf{A}_{II}\tau}\mathbf{B}_{II}\,d\tau = \mathbf{A}_{II}^{-1}\left(e^{\mathbf{A}_{II}\Delta T} - \mathbf{I}\right)\mathbf{B}_{II}, \text{ when } \mathbf{A}_{II}^{-1} \text{ exists} \end{aligned} \tag{12}$$

Note that the entries in the state vector $\mathbf{x}_S[k] \in \mathbb{R}^{2n\times 1}$ are grouped in the same sequence as in the vector $\mathbf{x}_{II}(t)$ described by Eq. (6):

$$\mathbf{x}_S[k] = [q_1[k] \quad \dot{q}_1[k] \quad q_2[k] \quad \dot{q}_2[k] \quad \ldots \quad q_n[k] \quad \dot{q}_n[k]]^{\mathrm{T}} \tag{13}$$

In this work, it is assumed that one step of time delay exists for the sensor measurement signal $\mathbf{m}[k]$, *i.e.* the feedback time delay is equal to one sampling period $\Delta T$. This is typically encountered when the dominant part of feedback delay is the communication time delay. The sensor noise vector is denoted as $\mathbf{w}_2[k] \in \mathbb{R}^{n_{w2}\times 1}$. To describe the one-step time delay and the addition of sensor noises, a simple discrete-time system can be defined as:

$$\begin{cases} \mathbf{x}_{TD}[k+1] = \mathbf{A}_{TD}\mathbf{x}_{TD}[k] + \mathbf{B}_{TD}\begin{bmatrix}\mathbf{m}[k] \\ \mathbf{w}_2[k]\end{bmatrix} \\ \mathbf{y}[k] = \mathbf{C}_{TD}\mathbf{x}_{TD}[k] + \mathbf{D}_{TD}\begin{bmatrix}\mathbf{m}[k] \\ \mathbf{w}_2[k]\end{bmatrix} \end{cases} \tag{14}$$

where

$$\mathbf{A}_{TD} = \mathbf{0},\ \mathbf{B}_{TD} = [\mathbf{I} \quad \mathbf{0}],\ \mathbf{C}_{TD} = \mathbf{I}, \text{ and } \mathbf{D}_{TD} = \begin{bmatrix}\mathbf{0} & s_{w_2}\mathbf{I}\end{bmatrix} \tag{15}$$

The input to this system is the original measurement signal $\mathbf{m}[k]$ and the sensor noise $\mathbf{w}_2[k]$, the output of the system is the delayed noisy signal $\mathbf{y}[k]$, which is the feedback signal to be used for control decisions. The formulation can be easily adapted and extended to model multiple steps of time delay, as well as different steps of time delay associated with different sensing channels. Parameter $s_{w2}$ is the scaling factor representing sensor noise level. Although the same scaling factor is assumed for all sensor noises in this formulation, a different factor can be assigned for each sensor noise entry, by replacing $s_{w2}\mathbf{I}$ in the above equation with a diagonal matrix that contains different diagonal entries.

While transmitting the delayed measurement signal $\mathbf{y}[k]$ to the controllers, this study is interested in decentralized feedback schemes. Figure 1 illustrates two decentralized feedback patterns for a five-story structure. It is assumed that at each floor $i$ ($i$ = 1, 2, …, 5), two measurement signals, $y_{2i\text{-}1}[k]$ and $y_{2i}[k]$, are acquired by sensors at that floor. In Figure 1(a), the feedback pattern is defined such that when making the decision for control device $u_i$, only measurement signals from

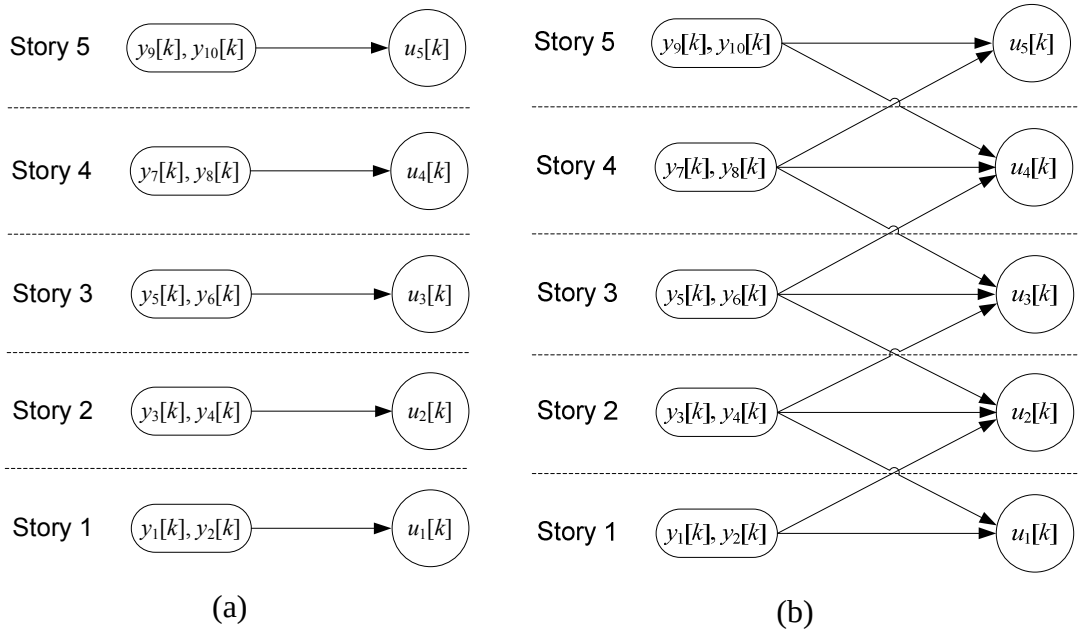


Figure 1. Decentralized feedback patterns: (a) fully decentralized with no information overlapping; (b) partially decentralized with information overlapping.

the *i*-th floor are needed. Figure 1(b) illustrates a partially decentralized feedback pattern with information overlapping. In this case, sensor measurements from neighboring floors (floor) are also available for making the control decision for control device $u_i$.

As illustrated in Figure 1(b), in decentralized feedback patterns with information overlapping, same sensor measurement signal may be utilized for the control decisions for multiple control devices. To represent information overlapping, one delayed measurement signal is repeated as multiple entries in $\mathbf{y}[k]$. Redundant rows are added into the definition of $\mathbf{y}[k]$ in Eq. (14); the entries in $\mathbf{y}[k]$ are then aggregated according to different information groups. For example, for the feedback pattern illustrated in Figure 1(b), the delayed sensor measurement signal $\mathbf{y}[k]$ is replaced by the new vector $\mathbf{y}_{repeat}$ defined in Figure 2. In this example, the length of the vector $\mathbf{y}_{repeat}$ is equal to twenty-six. This process of signal repeating is to facilitate later design of decentralized controllers that are uncoupled from each other.

The dynamical system that describes time delay and sensor noises (plus signal repeating in case

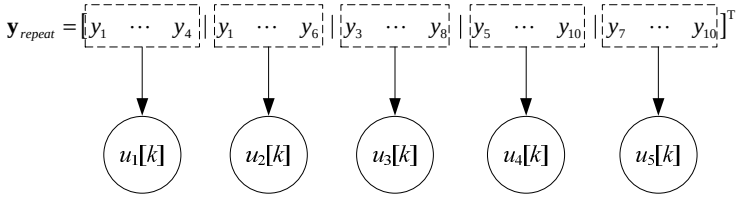


Figure 2. Redundant entries are used to represent signal repeating for decentralized feedback with information overlapping (Figure 1b).

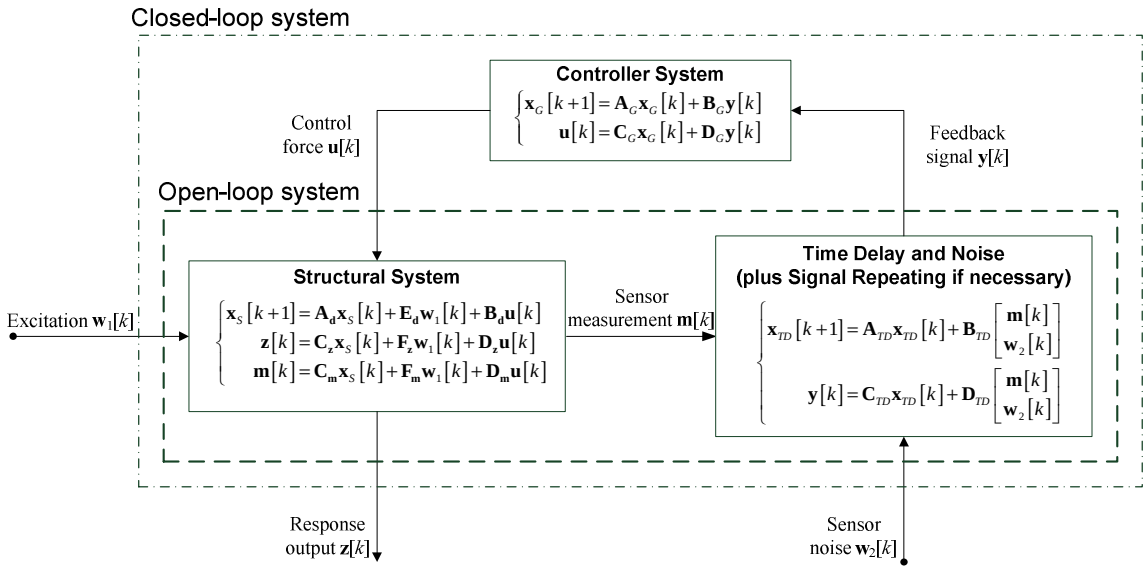


Figure 3. Diagram of the structural control system.

of information overlapping) is connected with the structural system in Eq. (11) to constitute the open-loop system depicted in Figure 3. Output of the structural system, i.e. the sensor measurement vector $\mathbf{m}[k]$, is an input to the time-delay system. For the overall open-loop system, the inputs include the excitation $\mathbf{w}_1[k]$, the sensor noises $\mathbf{w}_2[k]$, and the control forces $\mathbf{u}[k]$; outputs of the open-loop system include the structural response output $\mathbf{z}[k]$ and the feedback signals $\mathbf{y}[k]$. The number of state variables in the open-loop system is equal to the total number of state variables in the structural system and the time-delay system, *i.e.* $n_{OL} = 2n + n_{TD}$. Cascading the structural system and the time-delay system (e.g. using the `sysic` command in the Matlab Robust Control Toolbox [23]), the complete open-loop system is denoted as follows:

$$\begin{cases}\mathbf{x}[k+1]=\mathbf{A}\mathbf{x}[k]+\mathbf{B}_1\mathbf{w}[k]+\mathbf{B}_2\mathbf{u}[k]\\ \mathbf{z}[k]=\mathbf{C}_1\mathbf{x}[k]+\mathbf{D}_{11}\mathbf{w}[k]+\mathbf{D}_{12}\mathbf{u}[k]\\ \mathbf{y}[k]=\mathbf{C}_2\mathbf{x}[k]+\mathbf{D}_{21}\mathbf{w}[k]+\mathbf{D}_{22}\mathbf{u}[k]\end{cases} \tag{16}$$

where $\mathbf{w}[k]\in\mathbb{R}^{n_w\times 1}$ contains both the external excitation $\mathbf{w}_1[k]$ and the sensor noise $\mathbf{w}_2[k]$:

$$\mathbf{w}[k]=\begin{Bmatrix}\mathbf{w}_1[k]\\ \mathbf{w}_2[k]\end{Bmatrix} \tag{17}$$

The control objective is to design an effective feedback controller for the open-loop system with different feedback patterns. The controller takes the feedback signal $\mathbf{y}[k]$ as input, and outputs the control force vector $\mathbf{u}[k]$. Controller dynamics are described by the following state-space equations:

$$\begin{cases}\mathbf{x}_G[k+1]=\mathbf{A}_G\mathbf{x}_G[k]+\mathbf{B}_G\mathbf{y}[k]\\ \mathbf{u}[k]=\mathbf{C}_G\mathbf{x}_G[k]+\mathbf{D}_G\mathbf{y}[k]\end{cases} \tag{18}$$

In this study, it is assumed that both the controller and the open-loop system have the same number of states, *i.e.* $\mathbf{A}_G \in \mathbb{R}^{n_G \times n_G}$ and $n_G = n_{OL}$. For convenience, a matrix variable $\mathbf{G} \in \mathbb{R}^{(n_G+n_u)\times(n_G+n_y)}$ is defined to contain all controller parametric matrices:

$$\mathbf{G} = \begin{bmatrix} \mathbf{A}_G & \mathbf{B}_G \\ \mathbf{C}_G & \mathbf{D}_G \end{bmatrix} \tag{19}$$

## 3. Decentralized Discrete-time $\mathcal{H}_\infty$ Controller Design

For a decentralized controller design, the decentralized feedback can be represented by sparsity patterns in the controller matrices $\mathbf{A}_G$, $\mathbf{B}_G$, $\mathbf{C}_G$ and $\mathbf{D}_G$. For this purpose, entries in the feedback signal $\mathbf{y}[k]$ and the control force $\mathbf{u}[k]$ are divided into $N$ groups. While making control decisions for one group of control force entries, only one group of corresponding feedback signals is needed. Block-diagonal patterns are assigned to controller matrices in order to represent a decentralized control architecture that includes decentralized controllers $\mathbf{G}_I$, $\mathbf{G}_{II}$, …, and $\mathbf{G}_N$:

$$\begin{aligned} \mathbf{A}_G &= diag\left(\mathbf{A}_{G_I}, \mathbf{A}_{G_{II}}, \cdots, \mathbf{A}_{G_N}\right) \\ \mathbf{B}_G &= diag\left(\mathbf{B}_{G_I}, \mathbf{B}_{G_{II}}, \cdots, \mathbf{B}_{G_N}\right) \\ \mathbf{C}_G &= diag\left(\mathbf{C}_{G_I}, \mathbf{C}_{G_{II}}, \cdots, \mathbf{C}_{G_N}\right) \\ \mathbf{D}_G &= diag\left(\mathbf{D}_{G_I}, \mathbf{D}_{G_{II}}, \cdots, \mathbf{D}_{G_N}\right) \end{aligned} \tag{20}$$

Using the sparsity patterns shown in (20), the controller in Eq. (18) is equivalent to multiple uncoupled decentralized controllers, each controller requiring only one group of feedback signals to determine the control forces for that group:

$$\begin{cases} \mathbf{x}_{G_I}[k+1] = \mathbf{A}_{G_I}\mathbf{x}_{G_I}[k] + \mathbf{B}_{G_I}\mathbf{y}_I[k] \\ \mathbf{u}_I[k] = \mathbf{C}_{G_I}\mathbf{x}_{G_I}[k] + \mathbf{D}_{G_I}\mathbf{y}_I[k] \end{cases},$$

$$\cdots, \tag{21}$$

$$\begin{cases} \mathbf{x}_{G_N}[k+1] = \mathbf{A}_{G_N}\mathbf{x}_{G_N}[k] + \mathbf{B}_{G_N}\mathbf{y}_N[k] \\ \mathbf{u}_N[k] = \mathbf{C}_{G_N}\mathbf{x}_{G_N}[k] + \mathbf{D}_{G_N}\mathbf{y}_N[k] \end{cases}$$

As an example, for the fully decentralized feedback pattern shown in Figure 1(a), the total number of groups, $N$, is equal to five. Each feedback signal group contains two entries and each control force group has one entry. For the feedback pattern with information overlapping shown in Figure 1(b), the total number of groups is still equal to five and each control force group contains one entry; the feedback signals are aggregated as illustrated in Figure 2, which shows that feedback signal group $\mathbf{y}_I[k]$ has four entries, $\mathbf{y}_{II}[k]$, $\mathbf{y}_{III}[k]$, and $\mathbf{y}_{IV}[k]$ have six entries, and $\mathbf{y}_V[k]$ has four entries.

Assuming that the $\mathbf{D}_{22}$ matrix in the open-loop system in Eq. (16) is a zero matrix, following notations are defined [21]:

$$\left[\begin{array}{c|c|c} \tilde{\mathbf{A}} & \tilde{\mathbf{B}}_1 & \tilde{\mathbf{B}}_2 \\ \hline \tilde{\mathbf{C}}_1 & \tilde{\mathbf{D}}_{11} & \tilde{\mathbf{D}}_{12} \\ \hline \tilde{\mathbf{C}}_2 & \tilde{\mathbf{D}}_{21} & \end{array}\right] = \left[\begin{array}{cc|c|cc} \mathbf{A} & \mathbf{0} & \mathbf{B}_1 & \mathbf{0} & \mathbf{B}_2 \\ \mathbf{0} & \mathbf{0}_{n_G} & \mathbf{0} & \mathbf{I}_{n_G} & \mathbf{0} \\ \hline \mathbf{C}_1 & \mathbf{0} & \mathbf{D}_{11} & \mathbf{0} & \mathbf{D}_{12} \\ \hline \mathbf{0} & \mathbf{I}_{n_G} & \mathbf{0} & & \\ \mathbf{C}_2 & \mathbf{0} & \mathbf{D}_{21} & & \end{array}\right] \tag{22}$$

Zero submatrices with unspecified dimensions should have compatible dimensions with neighboring submatrices. Using the definitions above, the closed-loop system in Figure 3 can be formulated by concatenating the open-loop system with the controller system:

$$\begin{cases} \mathbf{x}_{CL}[k+1] = \mathbf{A}_{CL}\mathbf{x}_{CL}[k] + \mathbf{B}_{CL}\mathbf{w}[k] \\ \mathbf{z}[k] = \mathbf{C}_{CL}\mathbf{x}_{CL}[k] + \mathbf{D}_{CL}\mathbf{w}[k] \end{cases} \tag{23}$$

where

$$\mathbf{A}_{CL} = \tilde{\mathbf{A}} + \tilde{\mathbf{B}}_2\mathbf{G}\tilde{\mathbf{C}}_2, \mathbf{B}_{CL} = \tilde{\mathbf{B}}_1 + \tilde{\mathbf{B}}_2\mathbf{G}\tilde{\mathbf{D}}_{21}, \mathbf{C}_{CL} = \tilde{\mathbf{C}}_1 + \tilde{\mathbf{D}}_{12}\mathbf{G}\tilde{\mathbf{C}}_2, \mathbf{D}_{CL} = \tilde{\mathbf{D}}_{11} + \tilde{\mathbf{D}}_{12}\mathbf{G}\tilde{\mathbf{D}}_{21} \tag{24}$$

and **G** is as defined in Eq. (19). Note that the input to the closed-loop system is **w**[*k*], which contains the external excitation $\mathbf{w}_1[k]$ and sensor noises $\mathbf{w}_2[k]$, while the output is same as the structural output **z**[*k*] defined in Eq. (16). Using Z-transform [22], the dynamics of a discrete-time system can be represented by the transfer function $\mathbf{H}_{\mathbf{zw}}(z) \in \mathbb{C}^{n_z \times n_w}$ from disturbance **w** to output **z** as:

$$\mathbf{H}_{\mathbf{zw}}(z) = \mathbf{C}_{CL}\left(z\mathbf{I} - \mathbf{A}_{CL}\right)^{-1}\mathbf{B}_{CL} + \mathbf{D}_{CL} \tag{25}$$

The objective of $\mathcal{H}_\infty$ control is to minimize the $\mathcal{H}_\infty$-norm of the closed-loop discrete-time system, which in the frequency domain is defined as:

$$\left\|\mathbf{H}_{\mathbf{zw}}\right\|_\infty = \sup_{\omega \in [-\omega_N, \omega_N]} \bar{\sigma}\left[\mathbf{H}_{\mathbf{zw}}\left(e^{\mathrm{j}\omega\Delta T}\right)\right] \tag{26}$$

where $\omega$ represents angular frequency, $\omega_N = \pi/\Delta T$ is the Nyquist frequency, j is the imaginary unit, $\bar{\sigma}[\bullet]$ denotes the largest singular value of a matrix, and "sup" denotes the supremum (least upper bound) of a set of real numbers. The definition shows that in the frequency domain, the $\mathcal{H}_\infty$-norm of the system is equal to the peak of the largest singular value of the transfer function $\mathbf{H}_{\mathbf{zw}}\left(e^{\mathrm{j}\omega\Delta T}\right)$ in the Nyquist frequency range, i.e. the $\mathcal{H}_\infty$-norm represents the largest amplification gain from the disturbance **w** to the output **z**. Assume that the largest singular value reaches its peak when frequency $\omega$ is equal to $\omega_\mathrm{p}$, then the so called "worst-case" disturbance is a disturbance vector $\mathbf{w}(e^{\mathrm{j}\omega\Delta T})$ at frequency $\omega_\mathrm{p}$ and with the same direction as the right singular vector of the transfer function $\mathbf{H}_{\mathbf{zw}}\left(e^{\mathrm{j}\omega_\mathrm{p}\Delta T}\right)$ [24].

According to the Bounded Real Lemma, the following two statements are equivalent in specifying the performance criterion based on the $\mathcal{H}_\infty$-norm of a discrete-time system [25]:

1. The $\mathcal{H}_\infty$-norm of the system in Eq. (23) is less than $\gamma$, and $\mathbf{A}_{CL}$ is stable in the discrete-time sense (*i.e.* all of the eigenvalues of $\mathbf{A}_{CL}$ fall in the unit circle on the complex plane);
2. There exists a symmetric positive definite matrix $\mathbf{P} > 0$ such that the following matrix inequality holds:

$$\begin{bmatrix} -\mathbf{P}^{-1} & \mathbf{A}_{CL} & \mathbf{B}_{CL} & \mathbf{0} \\ * & -\mathbf{P} & \mathbf{0} & \mathbf{C}_{CL}^T \\ * & * & -\gamma\mathbf{I} & \mathbf{D}_{CL}^T \\ * & * & * & -\gamma\mathbf{I} \end{bmatrix} < 0 \tag{27}$$

where * denotes a symmetric entry, and "< 0" means that the matrix at the left side of the inequality is negative definite. Pre-multiplying and post-multiplying (27) by a positive definite matrix diag($\mathbf{P}, \mathbf{I}, \mathbf{I}, \mathbf{I}$), the congruence transformation leads to the following matrix inequality:

$$\begin{bmatrix} -\mathbf{P} & \mathbf{P}\mathbf{A}_{CL} & \mathbf{P}\mathbf{B}_{CL} & \mathbf{0} \\ * & -\mathbf{P} & \mathbf{0} & \mathbf{C}_{CL}^T \\ * & * & -\gamma\mathbf{I} & \mathbf{D}_{CL}^T \\ * & * & * & -\gamma\mathbf{I} \end{bmatrix} < 0 \tag{28}$$

Substituting the definitions in (24) into (28), we define a matrix variable **F** that is a function of **G** and **P**:

$$\mathbf{F}(\mathbf{G},\mathbf{P}) = \begin{bmatrix} -\mathbf{P} & \mathbf{P}\left(\tilde{\mathbf{A}} + \tilde{\mathbf{B}}_2\mathbf{G}\tilde{\mathbf{C}}_2\right) & \mathbf{P}\left(\tilde{\mathbf{B}}_1 + \tilde{\mathbf{B}}_2\mathbf{G}\tilde{\mathbf{D}}_{21}\right) & \mathbf{0} \\ * & -\mathbf{P} & \mathbf{0} & \left(\tilde{\mathbf{C}}_1 + \tilde{\mathbf{D}}_{12}\mathbf{G}\tilde{\mathbf{C}}_2\right)^T \\ * & * & -\gamma\mathbf{I} & \left(\tilde{\mathbf{D}}_{11} + \tilde{\mathbf{D}}_{12}\mathbf{G}\tilde{\mathbf{D}}_{21}\right)^T \\ * & * & * & -\gamma\mathbf{I} \end{bmatrix} \tag{29}$$

As a summary, the closed-loop $\mathcal{H}_\infty$-norm is less than $\gamma$ if $\mathbf{F}(\mathbf{G}, \mathbf{P}) < 0$. For a positive real number $\gamma$, the condition $\mathbf{F}(\mathbf{G}, \mathbf{P}) < 0$ is to be satisfied by searching for a decentralized controller **G (**with parametric structures illustrated in Eq. (20)) and a symmetric positive definite matrix **P**. Because both **G** and **P** are unknown variables, the problem has a bilinear matrix inequality (BMI) constraint [26]. When there is no sparsity requirements on matrix **G**, efficient algorithms and solvers are available for computing an ordinary controller matrix $\mathbf{G}_C$ [23; 25] that minimizes the closed-loop $\mathcal{H}_\infty$-norm:

$$\mathbf{G}_C = \begin{bmatrix} \mathbf{A}_{G_C} & \mathbf{B}_{G_C} \\ \mathbf{C}_{G_C} & \mathbf{D}_{G_C} \end{bmatrix} \tag{30}$$

In general, $\mathbf{A}_{G_C}$, $\mathbf{B}_{G_C}$, $\mathbf{C}_{G_C}$, and $\mathbf{D}_{G_C}$ are full matrices that represent centralized information feedback. When sparsity patterns (such as block-diagonal forms) in the controller parametric matrices are specified to achieve decentralized information feedback, off-the-shelf algorithms or numerical packages for solving the optimization problem with BMI constraints are not available [26; 27]. In this study, a heuristic homotopy method for designing continuous-time decentralized controllers, which was described by Zhai, *et al*. [21], is adapted for the discrete-time controller

design. Starting with a centralized controller, the homotopy method gradually transforms the controller into a decentralized one. The algorithm searches for a decentralized controller along the following homotopy path:

$$\mathbf{G} = (1-\lambda)\mathbf{G}_C + \lambda\mathbf{G}_D, 0 \le \lambda \le 1 \tag{31}$$

where $\lambda$ gradually increases from 0 to 1. $\mathbf{G}_C$ represents the initial centralized controller to start with and $\mathbf{G}_D$ the desired decentralized controller with the sparsity pattern shown in Eq. (20). Assume that a total number of $M$ steps are assigned for the homotopy path, and denote:

$$\lambda_k = k/M, k = 0,1,...,M \tag{32}$$

At every step $k$ along the homotopy path, the two matrix variables $\mathbf{G}_D$ and $\mathbf{P}$ are held constant one at a time, so that only one variable needs to be solved every time. In this way, the BMI constraint in Eq. (29) degenerates into a linear matrix inequality (LMI) constraint. For convenience, a matrix variable $\mathbf{V}$ is defined based on Eq. (29) as a function of variables $\mathbf{G}_D$, $\mathbf{P}$, and $\lambda$ (note that the centralized controller $\mathbf{G}_C$ is initially solved using conventional methods and remains constant during the homotopy search):

$$\mathbf{V}(\mathbf{G}_D, \mathbf{P}, \lambda) = \mathbf{F}(\mathbf{G}, \mathbf{P}) = \mathbf{F}\left((1-\lambda)\mathbf{G}_C + \lambda\mathbf{G}_D, \mathbf{P}\right) < 0 \tag{33}$$

At the beginning of every homotopy search, an upper bound for the closed-loop $\mathcal{H}_\infty$-norm, *i.e.* $\gamma$, is specified. The unknown variables in the above matrix inequality consist of $\mathbf{G}_D$ and $\mathbf{P}$ only. When $\mathbf{G}_D$ is held constant, a new $\mathbf{P}$ matrix can be computed for the next step; on the other hand, when $\mathbf{P}$ is held constant, a new $\mathbf{G}_D$ matrix is computed. If a homotopy search fails, $\gamma$ is increased by certain relaxation factor and a new search is conducted. The modified algorithm is described as follows:

[i] Compute a centralized controller $\mathbf{G}_C$ and the minimum closed-loop $\mathcal{H}_\infty$-norm $\gamma_C$ using existing robust control solvers [23; 25]; set $\gamma \leftarrow \gamma_C$, and set an upper limit ($\gamma_{\max}$) for $\gamma$, e.g. $10^6\gamma_C$.

[ii] Initialize $M$, the total number of homotopy steps, to be a positive number, e.g. $2^8$, and set an upper limit ($M_{\max}$) for $M$, e.g. $2^{13}$; Set $k \leftarrow 0$, $\lambda_0 \leftarrow 0$, and $\mathbf{G}_{D0} \leftarrow \mathbf{0}$; compute a feasible solution $\mathbf{P}_0$ under the constraint $\mathbf{V}(\mathbf{G}_{D0}, \mathbf{P}_0, \lambda_0) < 0$.

[iii] Set $k \leftarrow k+1$, and $\lambda_k \leftarrow k/M$; compute a solution $\mathbf{G}_D$ under the constraint $\mathbf{V}(\mathbf{G}_D, \mathbf{P}_{k-1}, \lambda_k) < 0$. If it is not feasible, go to Step [iv]. If $\mathbf{V}(\mathbf{G}_D, \mathbf{P}_{k-1}, \lambda_k) < 0$ is feasible, set $\mathbf{G}_{Dk} \leftarrow \mathbf{G}_D$, and compute a solution $\mathbf{P}$ under the constraint $\mathbf{V}\left(\mathbf{G}_{D_k}, \mathbf{P}, \lambda_k\right) < 0$. If $\mathbf{V}\left(\mathbf{G}_{D_k}, \mathbf{P}, \lambda_k\right) < 0$ is feasible, set $\mathbf{P}_k \leftarrow \mathbf{P}$, and go to Step [v]; if not, go to Step [vi].

[iv] Compute a solution $\mathbf{P}$ for $\mathbf{V}\left(\mathbf{G}_{D_{k-1}}, \mathbf{P}, \lambda_k\right) < 0$. If $\mathbf{V}\left(\mathbf{G}_{D_{k-1}}, \mathbf{P}, \lambda_k\right) < 0$ is not feasible, go to Step [vi]. If it is feasible, set $\mathbf{P}_k \leftarrow \mathbf{P}$ and compute a solution $\mathbf{G}_D$ under the constraint $\mathbf{V}(\mathbf{G}_D, \mathbf{P}_k, \lambda_k) < 0$. If $\mathbf{V}(\mathbf{G}_D, \mathbf{P}_k, \lambda_k) < 0$ is feasible, set $\mathbf{G}_{Dk} \leftarrow \mathbf{G}_D$ and go to Step [v]; if not, go to Step [vi].

[v] If $k < M$, go to Step [iii]. If $k$ is equal to $M$, $\mathbf{G}_{Dk}$ is the solution of the decentralized control problem, and the search ends here.

[vi] Set $M \leftarrow 2M$ under the constraint $M \le M_{\max}$ and restart the searching from Step [ii]. If $M$ reaches beyond $M_{\max}$, set $\gamma \leftarrow s_\gamma \gamma$ ($s_\gamma$ is a relaxation factor that is greater than one) under the constraint $\gamma \le \gamma_{\max}$ and restart from Step [ii]. If $\gamma$ exceeds $\gamma_{\max}$, it is concluded that the computation doesn't converge.

A decentralized controller is found when $k$ is equal to $M$ at step [v]. The controller has the property that the closed-loop $\mathcal{H}_\infty$-norm is less than $\gamma$. It should be pointed out that since the homotopy method is heuristic in nature, non-convergence in the computation does not imply that the decentralized $\mathcal{H}_\infty$ control problem has no solution.

## 4. Numerical Example

This section first illustrates procedures of the decentralized $\mathcal{H}_\infty$ controller design using a five-story example structure. Simulations are conducted to illustrate the effects of different feedback time delays for different decentralized feedback patterns. Performance of the decentralized $\mathcal{H}_\infty$ controllers is then compared with the performance of time-delayed decentralized controllers that are based on linear quadratic regulator (LQR) optimization criteria.

### 4.1. Formulation of the five-story example structure

A five-story model similar to the Kajima-Shizuoka Building is employed [28]. The building has a total height of about 19m (Figure 4a). As shown in Eq. (1), the five-story building is modeled as an in-plane lumped-mass structure with control devices allocated between every two neighboring floors. Figure 4b shows the model parameters of the lumped-mass structure. A discrete-time system describing the structural dynamics is formulated as shown in Eq. (11). Considering that excessive inter-story drifts are among the most damaging factors to building structures, the output matrices are defined as follows:

$$\mathbf{C}_\mathbf{z} = \begin{bmatrix} \mathbf{C}_{\mathbf{z}_1} \\ \hline \mathbf{C}_{\mathbf{z}_2} \end{bmatrix} = 1000 \times \left[\begin{array}{cccccccccc} 1 & & & & & & & & & \\ -1 & 0 & 1 & & & & & & & \\ & & -1 & 0 & 1 & & & & & \\ & & & & -1 & 0 & 1 & & & \\ & & & & & & -1 & 0 & 1 & 0 \\ \hline & & & & & \multicolumn{5}{c}{\mathbf{0}_{5\times 10}} \end{array}\right]_{10\times 10}, \quad \mathbf{F}_\mathbf{z} = \mathbf{0}, \quad \mathbf{D}_\mathbf{z} = \begin{bmatrix} \mathbf{D}_{\mathbf{z}_1} \\ \mathbf{D}_{\mathbf{z}_2} \end{bmatrix} = \begin{bmatrix} \mathbf{0}_{5\times 5} \\ \mathbf{I}_{5\times 5} \end{bmatrix} \times 10^{-3.5} \tag{34}$$

The assignments for $\mathbf{C}_\mathbf{z}$, $\mathbf{F}_\mathbf{z}$, and $\mathbf{D}_\mathbf{z}$ result in an output vector $\mathbf{z}[k] \in \mathbb{R}^{10\times 1}$ that can be partitioned into two sub-vectors:

$$\mathbf{z}[k] = \begin{Bmatrix} \mathbf{z}_1[k] \\ \mathbf{z}_2[k] \end{Bmatrix} = \begin{Bmatrix} \mathbf{C}_{\mathbf{z}_1}\mathbf{x}_S[k] \\ \mathbf{D}_{\mathbf{z}_2}\mathbf{u}[k] \end{Bmatrix} \tag{35}$$

Sub-vector $\mathbf{z}_1[k]$ contains entries related to structural response, and sub-vector $\mathbf{z}_2[k]$ contains entries related to control forces. The 2-norm of the output vector $\mathbf{z}[k]$ is a quadratic function of the inter-story drifts and the control forces:

$$\begin{aligned} \left\|\mathbf{z}[k]\right\|_2^2 &= \left\|\mathbf{C}_\mathbf{z}\mathbf{x}_S[k] + \mathbf{D}_\mathbf{z}\mathbf{u}[k]\right\|_2^2 \\ &= 10^6\left[q_1^2[k] + \left(q_2[k]-q_1[k]\right)^2 + \left(q_3[k]-q_2[k]\right)^2 + \left(q_4[k]-q_3[k]\right)^2 + \left(q_5[k]-q_4[k]\right)^2\right] \\ &\quad + 10^{-7}\left(u_1^2[k] + u_2^2[k] + u_3^2[k] + u_4^2[k] + u_5^2[k]\right) \end{aligned} \tag{36}$$

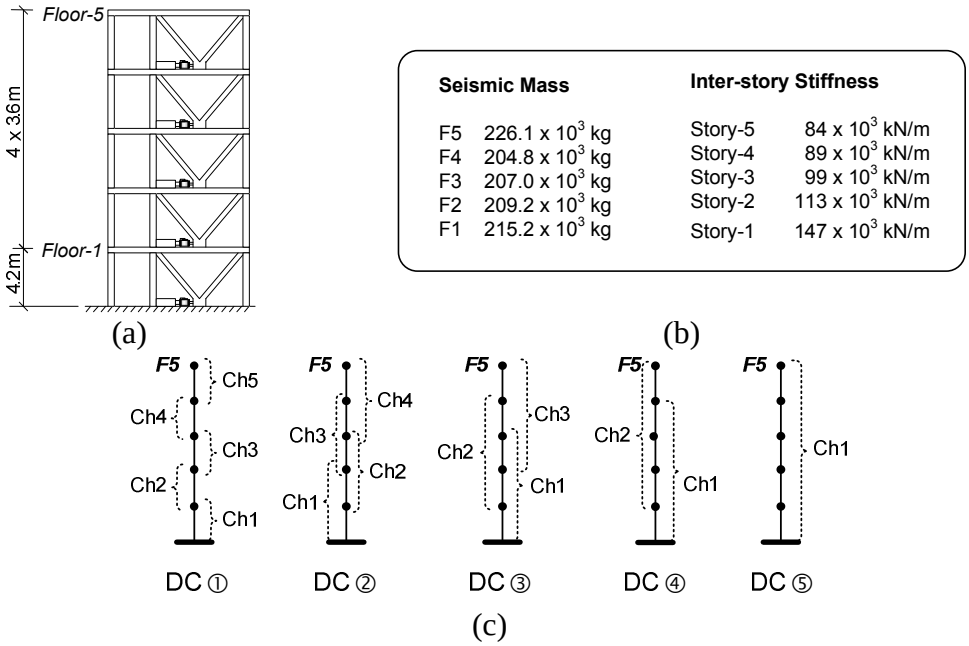


Figure 4. A five-story model similar to the Kajima-Shizuoka Building: (a) side elevation of the building; (b) model parameters of the lumped-mass structure; (c) communication subnet partitioning for different degrees of centralization (DC).

where $q_i[k]$ represents floor displacement relative to the ground (which means that $q_i[k]-q_{i-1}[k]$ for $i = 2 \ldots 5$ represents inter-story drift), and $u_i[k]$ represents control force. The $\mathcal{H}_\infty$ controller design aims to minimize the closed-loop $\mathcal{H}_\infty$-norm, which is defined as the system norm from the excitation input to the output $\mathbf{z}[k]$. The relative weighting between the structural response and the control effort is reflected by the magnitude of the output matrices, $\mathbf{C_z}$ and $\mathbf{D_z}$. If higher attenuation of structural response is needed, larger magnitude should be assigned to $\mathbf{C_z}$; on the contrary, if less control effort is available, larger magnitude should be assigned to $\mathbf{D_z}$.

It is assumed that inter-story drifts and velocities can be measured. Such an assumption is reasonable considering that modern control devices contain internal stroke sensors and load cells that measure real-time device displacements and forces, respectively [29]. Assuming a V-brace element is associated with the control device, the displacement and force measurements can be used to estimate inter-story drift and velocity. Accordingly, the measurement vector $\mathbf{m}[k]$ is defined as:

$$\mathbf{m}[k]=\left[q_1[k] \quad \dot{q}_1[k] \quad q_2[k]-q_1[k] \quad \dot{q}_2[k]-\dot{q}_1[k] \quad \cdots \quad q_5[k]-q_4[k] \quad \dot{q}_5[k]-\dot{q}_4[k]\right]^{\mathrm{T}} \qquad (37)$$

In order to obtain the above definition of $\mathbf{m}[k]$, the measurement matrices in Eq. (11) are determined as:

$$\mathbf{C_m} = \begin{bmatrix} 1 & & & & & & & & & \\ 0 & 1 & & & & & & & & \\ -1 & 0 & 1 & & & & & & & \\ & -1 & 0 & 1 & & & & & & \\ & & \ddots & \ddots & \ddots & & & & & \\ & & & & & & & & & \\ & & & & & & -1 & 0 & 1 & \end{bmatrix}_{10\times 10}, \ \mathbf{F_m} = \mathbf{0}, \ \mathbf{D_m} = \mathbf{0} \tag{38}$$

Sensor noise level $s_{w2}$ is set as 0.01 while constructing the time-delay system described in Eq. (14) and (15).

### 4.2. Controller designs with different feedback patterns

As illustrated in Figure 4c, the simulations are conducted for feedback patterns with different degrees of centralization (DC), which represents the number of neighboring floors that constitute a communication subnet and share their sensor data. The degree-of-centralization (DC) reflects the different communication architectures, with each communication subnet (as denoted by channels Ch1, Ch2, etc.) covering a limited number of stories. The controllers covered by a subnet are allowed to access the sensor data within that subnet. For example, case DC① implies each subnet consists of only one floor; since the inter-story drift and velocity on each floor are available for feedback, this communication pattern is the same as depicted in Figure 1(a). For case DC②, each subnet consists of two floors, resulting in four subnets for the five-story building; this communication pattern is the same as depicted in Figure 1(b), and the corresponding sensor measurement vector is as defined in Figure 2. For DC⑤, all five floors share their sensor data, resulting in a centralized information architecture. For stories covered by multiple overlapping subnets (such as in cases DC②, ③, and ④), each controller at these stories should have communication access to data within all the overlapping subnets. Although each controller may command multiple control devices, in this example, a control device can only be commanded by one controller.

A sampling period of 5 ms is first used for all (de)centralized feedback patterns; this implies that the feedback time delay is also set as 5 ms. The homotopy method is used to compute five decentralized controllers for case DC①: $\mathbf{G}_I^{①}$, $\mathbf{G}_{II}^{①}$, ..., $\mathbf{G}_V^{①}$, i.e. $N$ = 5 in Eq. (20). Each decentralized controller takes two feedback signals as input (*i.e.* inter-story drift and velocity at the story housing the decentralized controller), and outputs the desired control force at this story. For example, the decentralized controller $\mathbf{G}_I^{①}$, which has two input variables, four state variables, and one output variable, is determined by the homotopy search:

$$\mathbf{G}_I^{①} = \left[\begin{array}{c|c} \mathbf{A}_{\mathbf{G}_I^{①}} & \mathbf{B}_{\mathbf{G}_I^{①}} \\ \hline \mathbf{C}_{\mathbf{G}_I^{①}} & \mathbf{D}_{\mathbf{G}_I^{①}} \end{array}\right] = \left[\begin{array}{ccccc|c} 4.438\text{E-}04 & -2.117\text{E-}03 & 1.313\text{E-}03 & 4.975\text{E-}03 & -1.395\text{E-}02 & 1.387\text{E-}03 \\ -1.666\text{E-}03 & 2.042\text{E-}02 & -6.201\text{E-}03 & -2.784\text{E-}02 & 4.170\text{E-}02 & 5.704\text{E-}04 \\ 9.288\text{E-}04 & -4.616\text{E-}03 & 2.806\text{E-}03 & 1.003\text{E-}02 & -2.297\text{E-}02 & 1.874\text{E-}03 \\ 5.259\text{E-}03 & -3.244\text{E-}02 & 1.521\text{E-}02 & 6.962\text{E-}02 & -1.553\text{E-}01 & 1.082\text{E-}02 \\ \hline 1.860\text{E+}06 & -5.650\text{E+}06 & 6.525\text{E+}06 & 1.373\text{E+}07 & -8.270\text{E+}07 & 1.142\text{E+}07 \end{array}\right] \tag{39}$$

Note that the maximum magnitude of the eigenvalues of matrix $\mathbf{A}_{\mathbf{G}_I^{①}}$ is less than one, *i.e.* $\max\left(\left|eig\left(\mathbf{A}_{\mathbf{G}_I^{①}}\right)\right|\right)<1$. This ensures the numerical stability of the controller dynamics described in Eq. (21).

For the partially decentralized case DC②, five uncoupled decentralized controllers are computed as well. The dimensions of the five controllers are summarized in Table 1. The numbers of input/output variables correspond to the illustration in Figure 2.

Table 1 Dimensions of the decentralized dynamic controllers for feedback pattern DC②

| | $\mathbf{G}_I^{②}$ | $\mathbf{G}_{II}^{②}$ | $\mathbf{G}_{III}^{②}$ | $\mathbf{G}_{IV}^{②}$ | $\mathbf{G}_V^{②}$ |
|---|---|---|---|---|---|
| Input | 4 | 6 | 6 | 6 | 4 |
| State | 4 | 4 | 4 | 4 | 4 |
| Output | 1 | 1 | 1 | 1 | 1 |

Similarly, controllers for cases DC③ and DC④ have different dimensions. For the centralized case DC⑤, the centralized controller has ten input variables (*i.e.* inter-story drifts and velocities at all five stories), twenty state variables, and five output variables (*i.e.* five control forces).

Table 2 lists the open-loop $\mathcal{H}_\infty$-norm of the uncontrolled structure, as well as the closed-loop $\mathcal{H}_\infty$-norms $\|\mathbf{H}_{\mathbf{zw}}\|_\infty$ of the controlled structure. The $\mathcal{H}_\infty$-norm of the uncontrolled structure is computed using the discrete-time structural system defined in Eq. (11), while neglecting the control force vector **u** and the measurement vector **m**. Even with 5ms of time delay in the feedback loop, all controllers illustrate stable performance and achieve smaller $\mathcal{H}_\infty$-norm than the uncontrolled case, which indicates reduced "worst-case" amplification from the disturbance **w** to the output **z**. Also listed in Table 2 are the $\mathcal{H}_\infty$-norms $\|\mathbf{H}_{\mathbf{z}_1\mathbf{w}}\|_\infty$ from the disturbance **w** to the $\mathbf{z}_1$, i.e. the sub-vector $\mathbf{z}_1$ that accounts for structural response only as defined in Eq. (35). In this way, the reduction to the amplification from disturbance to structural response can be illustrated more clearly. Among the controlled cases, for either $\|\mathbf{H}_{\mathbf{zw}}\|_\infty$ or $\|\mathbf{H}_{\mathbf{z}_1\mathbf{w}}\|_\infty$, the centralized controller (case DC⑤) assumes that complete state information is available for control decisions for all five control devices; accordingly, the centralized controller achieves minimum closed-loop $\mathcal{H}_\infty$-norm (which means "best" control performance). In general, the higher the degree of centralization is, the smaller the $\mathcal{H}_\infty$-norm becomes.

Table 2 $\mathcal{H}_\infty$-norms of controlled (with 5ms feedback time delay) and uncontrolled structures

| | Uncontrolled | DC① | DC② | DC③ | DC④ | DC⑤ |
|---|---|---|---|---|---|---|
| $\|\mathbf{H}_{\mathbf{zw}}\|_\infty$ | 144.88 | 113.50 | 55.53 | 60.87 | 51.41 | 47.11 |
| $\|\mathbf{H}_{\mathbf{z}_1\mathbf{w}}\|_\infty$ | 144.88 | 47.27 | 25.96 | 27.27 | 18.59 | 17.87 |

### 4.3. Simulation results for $\mathcal{H}_\infty$ control cases

The 1995 Kobe NS (JMA Station) earthquake record with its peak acceleration scaled to 1m/s$^2$ is used as the ground excitation. Ideal actuators that generate any desired control forces are deployed at the five stories. In contrast to a realistic semi-active or active control device, an ideal actuator offers unlimited force capacity. To be consistent with the value of $s_{w2}$, sensor noises are injected as zero-mean normal distributions with a standard deviation that is 1% of the sensor signal amplitude.

Figure 5 illustrates the peak values of the inter-story drifts, absolute accelerations, and actuator forces for each story (floor). Compared with the uncontrolled case, all five controlled cases achieve significant reduction to structural response, and demonstrate stability with 5ms time delay in the feedback loop. The fully decentralized case without any information overlapping, case DC①, achieves similar reduction to inter-story drifts compared with the centralized case DC⑤, except for some difference at the 2nd story. Meanwhile, case DC① achieves much more reduction to peak floor accelerations and requires less actuator forces at the 3rd, 4th, and 5th stories. Other decentralized cases with information overlapping, including DC②, DC③, and

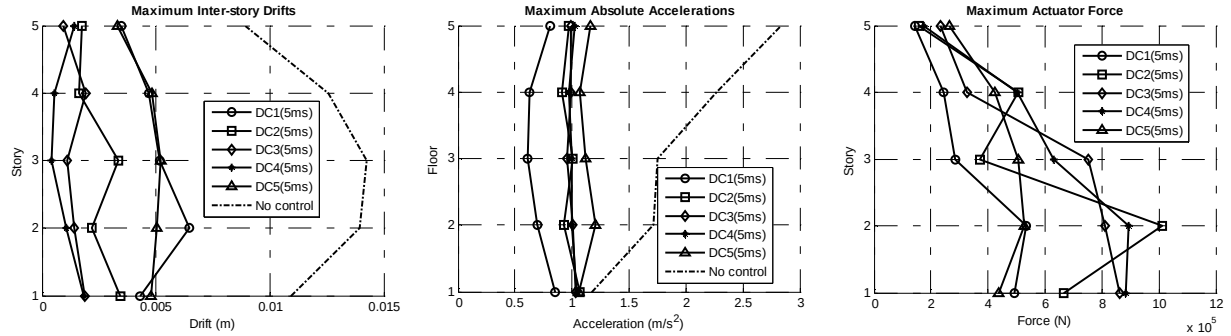


(a) (b) (c)

Figure 5. Simulation results for $\mathcal{H}_\infty$ control with 5ms time delay: (a) peak inter-story drifts; (b) peak absolute accelerations; (c) peak control forces

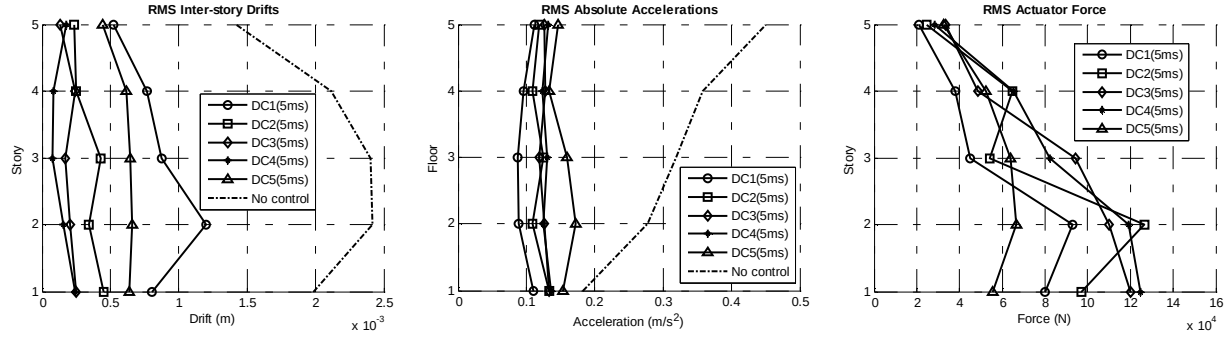


(a) (b) (c)

Figure 6. Simulation results for $\mathcal{H}_\infty$ control with 5ms time delay: (a) RMS inter-story drifts; (b) RMS absolute accelerations; (c) RMS control forces (note that the horizontal scales are different from these in Figure 5).

DC④, achieve more reduction to the peak drifts, while at the expense of larger peak control forces.

Figure 6 presents the root-of-mean-square (RMS) values of the inter-story drifts, absolute accelerations, and actuator forces for each story (floor). It is again illustrated that compared with the uncontrolled structure, significant reduction to inter-story drifts and floor accelerations has been achieved by all the control cases. Although case DC① achieves least reduction to RMS inter-story drifts, it achieves the most reduction to RMS floor accelerations. Similar to the peak value plots in Figure 5, Figure 6 shows that in general, cases DC②, DC③, and DC④, achieve more reduction to RMS inter-story drifts at the expense of larger control effort.

To illustrate the effect of different time delays due to different degrees of (de)centralization, additional simulations are conducted with different time delays adopted for five different feedback patterns (Table 3). For case DC①, where each actuator only requires sensor data at its own story to make control decisions, time delay is chosen to be the minimum as 5ms. For case DC②, where data from sensors on the actuator's own story and neighboring story (stories) are

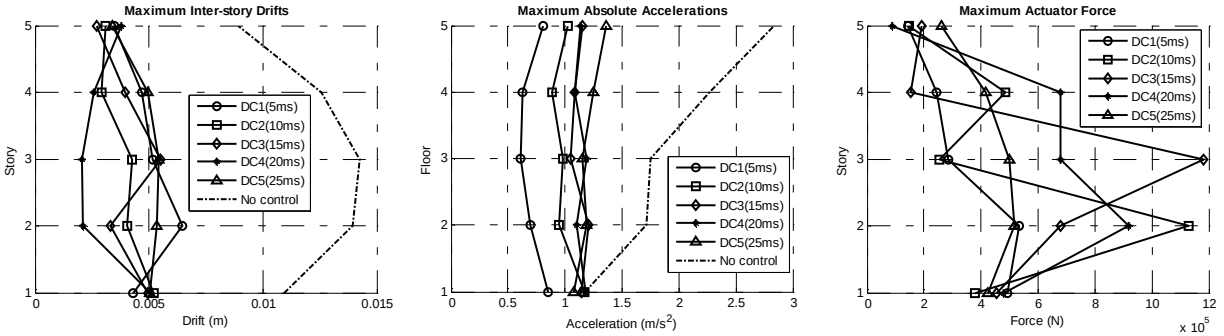


(a) (b) (c)

Figure 7. Simulation results for $\mathcal{H}_\infty$ control with different time delays: (a) peak inter-story drifts; (b) peak absolute accelerations; (c) peak control forces

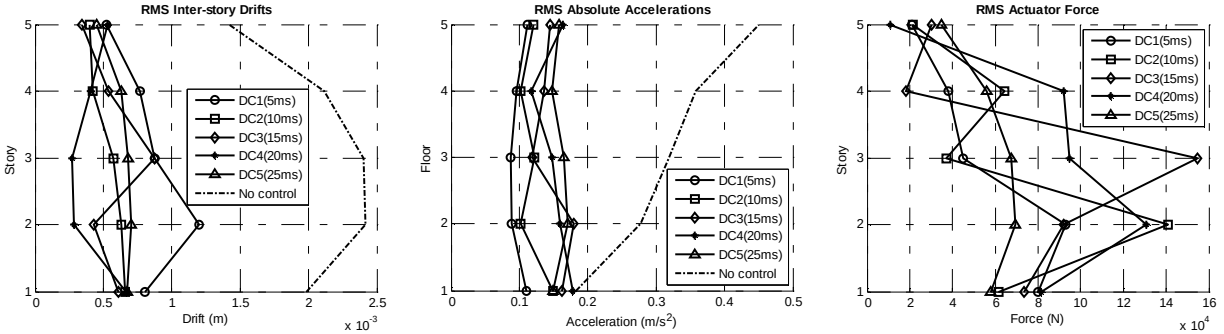


(a) (b) (c)

Figure 8. Simulation results for $\mathcal{H}_\infty$ control with different time delays: (a) RMS inter-story drifts; (b) RMS absolute accelerations; (c) RMS control forces (note that the horizontal scales are different from these in Figure 7).

required, time delay is adopted as 10ms. Similarly, for the cases DC③, DC④, and DC⑤, where more sensor data are required and processed, time delay is adopted as 15ms, 20ms, and 25ms, respectively. Using the newly computed controllers based on different time delays, simulated peak inter-story drifts and actuator forces are presented in Figure 7. Comparison between Figure 5 and Figure 7 shows that due to longer time delay, the performance of most control cases degrades while requiring larger actuator force capacities. In terms of reducing peak drifts and accelerations, all decentralized cases (DC① ~ DC④) offer comparable performance as the centralized case DC⑤. Although other decentralized cases have higher requirement on actuator capacity, DC① has lower requirement on overall actuator capacity than DC⑤. In addition, since decentralized case DC① has much lower requirement on the communication network, it can be more preferable for implementation. Similar trend can be observed in Figure 8 that illustrates the root-of-mean-square (RMS) values of the inter-story drifts, absolute accelerations, and actuator forces for each story (floor).

Table 3 Feedback time delays for five different feedback controllers

| | DC① | DC② | DC③ | DC④ | DC⑤ |
|---|---|---|---|---|---|
| Time delay (ms) | 5 | 10 | 15 | 20 | 25 |

### 4.4. Comparison with decentralized controllers based on the LQR optimization criteria

It could be instructive to compare the decentralized $\mathcal{H}_\infty$ controller design with the decentralized LQR controller design that was previously studied [10]. The LQR control algorithm aims to select the optimal control force trajectory **u** by minimizing the expected value of a quadratic cost function, $J$:

$$J = \sum_{k=l}^{\infty} \left( \mathbf{x}^{\mathrm{T}}[k]\mathbf{Q}\mathbf{x}[k] + \mathbf{u}^{\mathrm{T}}[k-l]\mathbf{R}\mathbf{u}[k-l] \right),\ \mathbf{Q}_{2n\times 2n} \geq 0 \text{ and } \mathbf{R}_{n_u \times n_u} > 0 \tag{40}$$

where $l$ denotes the number of feedback delay steps, which is set to one in this work. Using the same definition of the output matrices $\mathbf{C}_\mathbf{z}$ and $\mathbf{D}_\mathbf{z}$ as described in Eq. (34), the following weighting matrices are employed for the LQR controller design:

$$\mathbf{Q} = \mathbf{C}_\mathbf{z}{}^{\mathrm{T}}\mathbf{C}_\mathbf{z}, \quad \mathbf{R} = \mathbf{D}_\mathbf{z}{}^{\mathrm{T}}\mathbf{D}_\mathbf{z} \tag{41}$$

As a result, the LQR optimization index $J$ is approximately proportional to the signal 2-norm of the system output:

$$\begin{aligned} J &= \sum_{k=1}^{\infty} \left( \mathbf{x}^{\mathrm{T}}[k]\mathbf{C}_\mathbf{z}{}^{\mathrm{T}}\mathbf{C}_\mathbf{z}\mathbf{x}[k] + \mathbf{u}^{\mathrm{T}}[k-1]\mathbf{D}_\mathbf{z}{}^{\mathrm{T}}\mathbf{D}_\mathbf{z}\mathbf{u}[k-1] \right) \\ &\approx \sum_{k=1}^{\infty} \left\| \mathbf{C}_\mathbf{z}\mathbf{x}[k] + \mathbf{D}_\mathbf{z}\mathbf{u}[k] \right\|_2^2 \\ &= \sum_{k=1}^{\infty} \left\| \mathbf{z}[k] \right\|_2^2 \\ &= \left\| \mathbf{z} \right\|_2^2 / \Delta T \end{aligned} \tag{42}$$

where $\Delta T$ is the sampling period, and note that $\mathbf{C}_\mathbf{z}{}^{\mathrm{T}}\mathbf{D}_\mathbf{z} = \mathbf{0}$ and $\mathbf{D}_\mathbf{z}{}^{\mathrm{T}}\mathbf{C}_\mathbf{z} = \mathbf{0}$ using the definitions in Eq. (34). With feedback time delay considered in the above formulation, the design of the LQR controller iteratively searches for an optimal control gain matrix by traversing along the

optimization gradient. Sparsity shape constraints are iteratively applied to the search gradient in order to compute the decentralized gain matrices. Since the LQR control approach is equivalent to an $\mathcal{H}_2$ control design that minimizes the closed-loop $\mathcal{H}_2$-norm from the ground excitation $\mathbf{w}_1$ to the system output $\mathbf{z}$, LQR controllers are expected to perform well in reducing the closed-loop $\mathcal{H}_2$-norm $\left\|\mathbf{H}_{\mathbf{zw}_1}\right\|_2$ [24; 30]. Similar to the $\mathcal{H}_\infty$ norm, the $\mathcal{H}_2$-norm of a discrete-time system can also be written in terms of the singular values of the transfer function matrix:

$$\left\|\mathbf{H}_{\mathbf{zw}_1}\right\|_2 = \sqrt{\frac{\Delta T}{2\pi}\int_{-\omega_N}^{+\omega_N}\sum_i \sigma_i^2\left[\mathbf{H}_{\mathbf{zw}_1}\left(e^{\mathrm{j}\omega\Delta T}\right)\right]d\omega} \tag{43}$$

In this example, the second dimension of the transfer function matrix $\mathbf{H}_{\mathbf{zw}_1}\left(e^{\mathrm{j}\omega\Delta T}\right)$ is one, because the disturbance $\mathbf{w}_1$ is a scalar that represents the ground excitation. Therefore, $\mathbf{H}_{\mathbf{zw}_1}\left(e^{\mathrm{j}\omega\Delta T}\right)$ has only one singular value at each frequency $\omega$, which is the largest singular value.

Figure 9 compares the singular values of the closed-loop transfer function $\mathbf{H}_{\mathbf{zw}_1}\left(e^{\mathrm{j}\omega\Delta T}\right)$ for cases using (de)centralized $\mathcal{H}_\infty$ controllers and using (de)centralized LQR controllers, with 5ms feedback time delay considered. The peak singular value of each $\mathcal{H}_\infty$ control case is less than the peak singular values of the corresponding LQR control case with the same DC. The closest pair is for case DC1, where the peak singular value is equal to 81.8 using the decentralized $\mathcal{H}_\infty$ controller, and equal to 84.6 using the decentralized LQR controller. This shows that decentralized $\mathcal{H}_\infty$ controllers perform better at "pushing down the peak of the largest singular value over the frequency span," which agrees with the objective of minimizing the closed-loop $\mathcal{H}_\infty$-norms (as defined in Eq. (26)). On the other hand, the area covered under the singular value curve of each LQR control case is less than the area covered under the singular value curve of the corresponding $\mathcal{H}_\infty$ control case with the same DC. This shows that the decentralized LQR

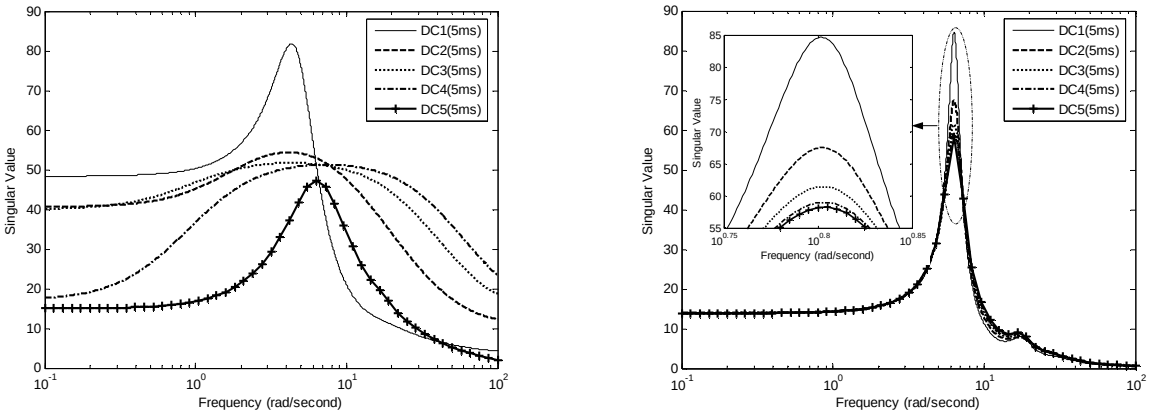


(a) Time-delayed $\mathcal{H}_\infty$ controllers (b) Time-delayed LQR controllers

Figure 9. Singular values of closed-loop transfer functions $\mathbf{H}_{\mathbf{zw}_1}\left(e^{\mathrm{j}\omega\Delta T}\right)$

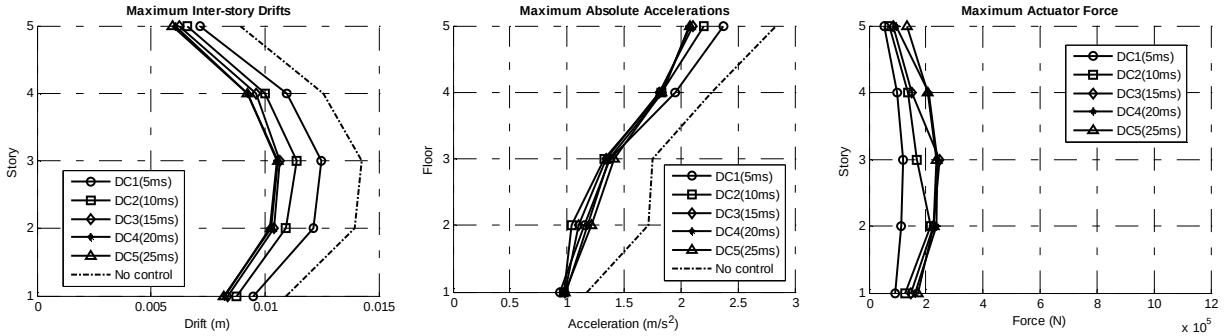


(a) (b) (c)

Figure 10. Simulation results for LQR control with different time delays: (a) peak inter-story drifts; (b) peak absolute accelerations; (c) peak control forces

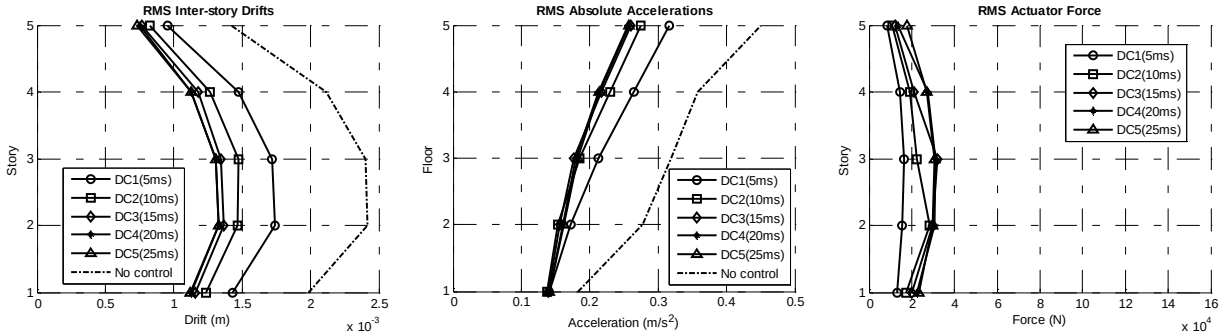


(a) (b) (c)

Figure 11. Simulation results for LQR control with different time delays: (a) RMS inter-story drifts; (b) RMS absolute accelerations; (c) RMS control forces (note that the horizontal scales are different from these in Figure 10).

controllers perform better at "reducing all singular values over the frequency span," which agrees with the objective of minimizing the $\mathcal{H}_2$ norm (as defined in Eq. (43)).

To illustrate the effect of different time delays due to different degrees of (de)centralization, simulations are conducted with different time delays adopted for the LQR controllers with the five different feedback patterns shown in Table 3. The same 1995 Kobe NS (JMA Station) earthquake record is scaled to a peak acceleration of 1m/s$^2$; ideal actuators are again deployed at all five stories. Simulated peak inter-story drifts, absolute accelerations, and actuator forces are presented in Figure 10, and RMS values are presented in Figure 11. These two figures are comparable to Figure 7 and Figure 8, where $\mathcal{H}_\infty$ controllers with different time delays are adopted. The comparison shows that in this example, the LQR controllers entail less control effort, while achieving less reduction to peak drifts and absolute accelerations.

## 5. Summary and Discussion

This paper proposes a decentralized controller design that aims to minimize the closed-loop $\mathcal{H}_\infty$ norm of a controlled civil structure. The design is formulated in discrete-time domain, and

considers possible feedback time delay. The decentralized controller design employs a homotopy method, which gradually transforms an original centralized controller into uncoupled decentralized ones. LMI constraints describing the closed-loop $\mathcal{H}_\infty$ norm performance are ensured at each homotopy step. Such solutions are necessary to provide control systems with the ability to scale with the number of sensors and actuators implemented in the system. Nevertheless, it should be noted that the homotopy approach for decentralized $\mathcal{H}_\infty$ controller design is heuristic. The approach may not guarantee the minimum $\mathcal{H}_\infty$-norm over the complete solution space.

Performance of the time-delayed decentralized $\mathcal{H}_\infty$ controller design is validated through a number of numerical simulations using a five-story structure. It is shown that with less feedback latency, decentralized control strategies may achieve similar performance when compared with centralized ones. Therefore, decentralized strategies can be more appealing due to the lower cost of implementing a decentralized communication network. Comparison between the decentralized $\mathcal{H}_\infty$ controllers and the decentralized LQR-based controllers illustrates that both controllers deliver expected performance in terms of reducing closed-loop system norms. The trade-off between structural response attenuation and control effort is demonstrated for both the $\mathcal{H}_\infty$ controllers and LQR controllers. Since the proposed control design is based on the assumption of system linearity, further study is needed on how to improve the control performance with non-linear control devices. Future investigation may also develop a systematic method for the design of decentralized architectures, e.g., the delineation of overlapping subnets, as well as the selection of appropriate degrees of centralization.

## 6. Acknowledgement

The author appreciates the insightful opinions to this study provided by Prof. Kincho H. Law of the Department of Civil and Environmental Engineering at Stanford University, and by Prof. Sanjay Lall of the Department of Aeronautics and Astronautics at Stanford University.

## References

[1] Soong TT. *Active Structural Control: Theory and Practice.* Wiley: Harlow, Essex, England, 1990.

[2] Spencer BF, Jr. and Nagarajaiah S. State of the art of structural control. *Journal of Structural Engineering* 2003; **129** (7): 845-856.

[3] Yao JTP. Concept of structural control. *Journal of Structural Division, ASCE* 1972; **98** (7): 1567-1574.

[4] Housner GW, Bergman LA, Caughey TK, Chassiakos AG, Claus RO, Masri SF, Skelton RE, Soong TT, Spencer BF, Jr. and Yao JTP. Structural control: past, present, and future. *Journal of Engineering Mechanics* 1997; **123** (9): 897-971.

[5] Chu SY, Soong TT and Reinhorn AM. *Active, Hybrid, and Semi-active Structural Control: a Design and Implementation Handbook.* Wiley: Hoboken, NJ, 2005.

[6] Soong TT and Spencer BF, Jr. Supplemental energy dissipation: state-of-the-art and state-of-the-practice. *Engineering Structures* 2002; **24** (3): 243-259.

[7] Siljak DD. *Decentralized Control of Complex Systems.* Academic Press: Boston, 1991.

[8] Lunze J. *Feedback Control of Large Scale Systems.* Prentice-Hall: Englewood Cliffs, NJ, 1992.
[9] Sandell N, Jr., Varaiya P, Athans M and Safonov M. Survey of decentralized control methods for large scale systems. *Automatic Control, IEEE Transactions on* 1978; **23** (2): 108-128.
[10] Wang Y, Swartz RA, Lynch JP, Law KH, Lu K-C and Loh C-H. Decentralized civil structural control using real-time wireless sensing and embedded computing. *Smart Structures and Systems* 2007; **3** (3): 321-340.
[11] Balandin DV and Kogan MM. LMI-based optimal attenuation of multi-storey building oscillations under seismic excitations. *Structural Control and Health Monitoring* 2005; **12** (2): 213-224.
[12] Chase JG and Smith HA. Robust $H_\infty$ control considering actuator saturation. I: theory. *Journal of Engineering Mechanics* 1996; **122** (10): 976-983.
[13] Lin C-C, Chang C-C and Chen H-L. Optimal $H_\infty$ output feedback control systems with time delay. *Journal of Engineering Mechanics* 2006; **132** (10): 1096-1105.
[14] Mahmoud MS, Terro MJ and Abdel-Rohman M. An LMI approach to $H_\infty$-control of time-delay systems for the benchmark problem. *Earthquake Engineering & Structural Dynamics* 1998; **27** (9): 957-976.
[15] Johnson EA, Voulgaris PG and Bergman LA. Multiobjective optimal structural control of the Notre Dame building model benchmark. *Earthquake Engineering & Structural Dynamics* 1998; **27** (11): 1165-1187.
[16] Wang S-G. Robust active control for uncertain structural systems with acceleration sensors. *Journal of Structural Control* 2003; **10** (1): 59-76.
[17] Yang JN, Lin S and Jabbari F. $H_\infty$-based control strategies for civil engineering structures. *Structural Control and Health Monitoring* 2004; **11** (3): 223-237.
[18] Chase JG, Smith HA and Suzuki T. Robust $H_\infty$ control considering actuator saturation. II: applications. *Journal of Engineering Mechanics* 1996; **122** (10): 984-993.
[19] Boyd S, El Ghaoui L, Feron E and Balakrishnan V. *Linear Matrix Inequalities in System and Control Theory.* SIAM: Philadelphia, PA, 1994.
[20] Wang Y, Lynch JP and Law KH. Decentralized $H_\infty$ controller design for large-scale civil structures. *Earthquake Engineering & Structural Dynamics* 2009; **38** (3): 377-401.
[21] Zhai G, Ikeda M and Fujisaki Y. Decentralized $H_\infty$ controller design: a matrix inequality approach using a homotopy method. *Automatica* 2001; **37** (4): 565-572.
[22] Franklin GF, Powell JD and Workman ML. *Digital Control of Dynamic Systems.* Addison-Wesley: Menlo Park, CA, 1998.
[23] Chiang RY and Safonov MG. *MATLAB robust control toolbox.* MathWorks, Inc.: Natick, MA, 1998.
[24] Skogestad S and Postlethwaite I. *Multivariable Feedback Control: Analysis and Design.* John Wiley: Chichester, West Sussex, England, 2005.
[25] Gahinet P and Apkarian P. A linear matrix inequality approach to $H_\infty$ control. *International Journal of Robust and Nonlinear Control* 1994; **4** (4): 421-448.
[26] VanAntwerp JG and Braatz RD. A tutorial on linear and bilinear matrix inequalities. *Journal of Process Control* 2000; **10** (4): 363-385.

[27] Goh KC, Safonov MG and Papavassilopoulos GP. A global optimization approach for the BMI problem. *Proceedings of the 33rd IEEE Conference on Decision and Control*. **3**: 2009-2014, Lake Buena Vista, FL, USA, December 14-16, 1994.
[28] Kurata N, Kobori T, Takahashi M, Niwa N and Midorikawa H. Actual seismic response controlled building with semi-active damper system. *Earthquake Engineering & Structural Dynamics* 1999; **28** (11): 1427-1447.
[29] Kurino H, Tagami J, Shimizu K and Kobori T. Switching oil damper with built-in controller for structural control. *Journal of Structural Engineering* 2003; **129** (7): 895-904.
[30] Burl JB. *Linear optimal control : $H_2$ and $H_\infty$ methods.* Addison Wesley Longman: Menlo Park, CA, 1999.